Time-dependent density-functional theory simulation of local currents in pristine and single-defect zigzag graphene nanoribbons

Shenglai He,[a] Arthur Russakoff, Yonghui Li, and Kálmán Varga[b]
Department of Physics and Astronomy, Vanderbilt University, Nashville, Tennessee 37235, USA

(Received 15 April 2016; accepted 7 July 2016; published online 21 July 2016)

The spatial current distribution in H-terminated zigzag graphene nanoribbons (ZGNRs) under electrical bias is investigated using time-dependent density-functional theory solved on a real-space grid. A projected complex absorbing potential is used to minimize the effect of reflection at simulation cell boundary. The calculations show that the current flows mainly along the edge atoms in the hydrogen terminated pristine ZGNRs. When a vacancy is introduced to the ZGNRs, loop currents emerge at the ribbon edge due to electrons hopping between carbon atoms of the same sublattice. The loop currents hinder the flow of the edge current, explaining the poor electric conductance observed in recent experiments. *Published by AIP Publishing.*
[http://dx.doi.org/10.1063/1.4959088]

I. INTRODUCTION

Graphene is a two-dimensional material which has attracted considerable interest due to its superior electronic and mechanical properties.[1] Graphene does not have a bandgap and limits its potential application in nano-electronic devices. Alternatively, Graphene nanoribbons (GNRs) have a bandgap which is opened by the lateral confinement. This makes them promising materials for future nanoscale applications.[2–10] Currently, there are several methods to fabricate graphene nanoribbons such as chemical vapor deposition,[5,6] gas-phase chemical/plasma etching,[3] and oxidized unzipping of carbon nanotubes.[6,11–13] However, the measured electronic properties of GNRs have an apparent dependency on the experimental process.[2,4,5] This may be explained by the difficulty in producing pristine graphene free of defects.[2,6]

An understanding of the local current distribution in electrically biased GNRs, and how this distribution is affected by defects, is desirable to interpret the measured transport properties. Recently, experimental methods have been developed to image the local current. Stützel *et al.*[14] investigated local currents in GNRs through scanning photocurrent microscopy, and Lubk *et al.*[15] measured local currents in solids with atomic resolution using transmission electron microscopy. Negative local resistance has been experimentally observed in GNRs at the low temperature limit and interpreted using a simple viscous Fermi liquid model of the local current.[16]

Although there are many theoretical work on the transmission property of GNRs,[17–22] theoretical investigations of local current are rare and typically use tight-binding models which only consider interactions with nearest neighbors.[23,24] In these studies, only bond currents can be examined, while electron hopping between non-bonded atoms is neglected. Solomon *et al.*[25] included a coupling between second-nearest neighbor atoms in the study of local currents in molecular junctions and found that current flow through non-bonded atoms dominates in some instances. Since current flow is the result of electron interference between all possible electron transport channels, first principles calculation is needed which includes a more complete electron interactions. In Ref. 26, the local current density in pristine armchair graphene nanoribbons with varying width has been investigated using ab initio calculations, and streamline currents have been observed. The effect of edge hydrogenation and oxidation on the transport of zigzag nanoribbons has been studied in Ref. 27, and spin polarization has been predicted. These examples show the rich physics problems accessible with first principles and/or experimental studies of nanoribbons.

In this work, we investigate the local current under a bias voltage in both pristine and single-vacancy H-terminated zigzag GNRs (ZGNRs) at *ab initio* level using the time-dependent density-functional theory (TDDFT).[28] The nonequilibrium Green's function approach (NEGF),[29–31] combined with the density functional theory (DFT)[32] Hamiltonian is the most popular approach to describe steady state electron transport in nanostructures. This approach, however, is a manifestly ground state theory (it is based on the ground state Kohn-Sham single particle states) and alternative schemes using TDDFT are proposed.[33–47] The TDDFT is a computationally feasible approach to access excitation energies, and it is expected to give a better description of the nonequilibrium current carrying states than the conventional DFT. The apparent advantage of the TDDFT scheme is that it is readily usable for time dependent problems. In an earlier work, we have compared the TDDFT and NEGF-DFT approaches for calculation of transport properties of molecular junctions and discussed the differences of the two approaches.[48] One advantage of the TDDFT approach is that it only needs a single time propagation, while in NEGF-DFT, one needs converged calculation for many energies to calculate the current. At the same time, NEGF-DFT is evidently time independent, while the TDDFT approach has a transient period before the time-independent limit is reached. Another drawback of the TDDFT approach is that it only works for finite bias, and zero bias conductance cannot be easily calculated with that approach.

[a]shenglai.he@vanderbilt.edu
[b]kalman.varga@vanderbilt.edu

The paper is organized as follows. In Sec. II, we present the theoretical method. In Sec. III, we present the calculation of the electron transport for the pristine and single-vacancy ZGNRs and interpret the results by investigating the local current distribution. Finally, in Sec. IV, the paper is closed with a summary and future outlook.

II. FORMALISM

The current flow in pristine and single-vacancy ZGNRs under a bias voltage is simulated using TDDFT[49] on a real-space grid with real-time propagation. A rectangular simulation box with zero-boundary condition is used. The initial ground state of the system is prepared by performing a density functional theory calculation. The electronic dynamics are described by the time-dependent Kohn-Sham equation

$$i\hbar\frac{\partial\psi_k(\mathbf{r},t)}{\partial t}=H\psi_k(\mathbf{r},t),\quad k=1,\ldots,N, \tag{1}$$

where ψ_k is the time-dependent single-particle Kohn-Sham orbitals, H is the Kohn-Sham Hamiltonian, and N is the number of occupied orbitals. The total electron density is defined by a sum over all occupied orbitals

$$\rho(\mathbf{r},t)=\sum_{k=1}^{N}2|\psi_k(\mathbf{r},t)|^2, \tag{2}$$

where each orbital is initially occupied by 2 electrons. The Hamiltonian, H, in Eq. (1) is given by

$$H=-\frac{\hbar^2}{2m}\nabla_{\mathbf{r}}^2+V_{\mathrm{A}}(\mathbf{r})+V_{\mathrm{H}}[\rho](\mathbf{r},t)+V_{\mathrm{XC}}[\rho](\mathbf{r},t)+V_{\mathrm{ext}}(\mathbf{r},t), \tag{3}$$

where V_{A} is the ionic core potential, V_{H} is the Hartree potential, V_{XC} is the exchange-correlation potential, and $V_{\mathrm{ext}}(\mathbf{r},t)$ is the time-dependent external potential. V_{A} is a sum of norm-conserving pseudopotentials of the form given by Troullier-Martins[50] centered at each ion. The Hartree potential, V_{H}, is given by

$$V_{\mathrm{H}}(\mathbf{r},t)=\int d\mathbf{r}'\frac{\rho(\mathbf{r}',t)}{|\mathbf{r}-\mathbf{r}'|}, \tag{4}$$

and accounts for the electrostatic Coulomb interaction between electrons. Eq. (4) is computed by numerically solving the Poisson equation. To represent the exchange–correlation potential, V_{XC}, we employ the adiabatic local–density approximation (ALDA) with the parameterization of Perdew and Zunger.[51] In this study, $V_{\mathrm{ext}}(\mathbf{r},t)$ is a slowly ramped bias potential. The external bias potential is defined as

$$V_{\mathrm{ext}}(\mathbf{r},t)=\begin{cases}f(t)\dfrac{\mathrm{V_b}}{2}, & \mathbf{r}\in\text{left electrode}\\ 0, & \mathbf{r}\in\text{central region}\\ -f(t)\dfrac{\mathrm{V_b}}{2}, & \mathbf{r}\in\text{right electrode},\end{cases} \tag{5}$$

where V_{b} is a constant. The local current is investigated within the central region. The ramp function, $f(t)$, is given by

$$f(t)=\begin{cases}\dfrac{t}{\tau}, & t\le\tau\\ 1, & t>\tau,\end{cases} \tag{6}$$

where $\tau=0.5$ fs is the ramp time. The time-dependent Kohn-Sham orbitals may be formally propagated from the initial state to some time, t, by using the time–evolution operator

$$U(0,t)=\mathcal{T}\exp\left[-\frac{i}{\hbar}\int_0^t H(\mathbf{r},t')dt'\right], \tag{7}$$

where $\mathcal{T}$ denotes time ordering. In practice, $U(t,0)$ is split into a product of multiple short-time propagators

$$U(0,t)=\prod_q U(t_q,t_q+\delta t),\quad t_q=q\delta t, \tag{8}$$

which evolve the Kohn-Sham orbitals from t_q to $t_q+\delta t$. The short-time propagator is defined by

$$U(t_q,t_q+\delta t)=\exp\left[-\frac{i\delta t}{\hbar}H(\mathbf{r},t_q)\right]. \tag{9}$$

The time step, δt, is chosen to be sufficiently small so that the Hamiltonian can be treated as constant. A fourth-order Taylor expansion is used to approximate Eq. (9)

$$U(t_q,t_q+\delta t)\approx\sum_{n=0}^{4}\frac{1}{n!}\left(-\frac{i\delta t}{\hbar}H(\mathbf{r},t_q)\right)^n. \tag{10}$$

Given a sufficiently small time step, this method provides excellent accuracy with reasonable computational cost.[52–55]

As the bias potential drives electron current to the boundary of the simulation cell, the zero-boundary condition used in our simulations will lead to an unphysical reflection. To avoid this effect, a complex absorbing potential (CAP) of the form given by Manolopoulos[56] is added in the region close to the boundary. In the present calculation, the CAP would reduce the electron density in the electrode regions and, through the Hartree and exchange-correlation potentials, affect the Kohn-Sham orbitals in the region where the CAP is zero. To solve this problem, we have implemented the method proposed in Ref. 48, where the CAP potential (W) is multiplied by a projector P

$$W\rightarrow PWP. \tag{11}$$

The projector is given by

$$P=1-\sum_{i=1}^{N}|\psi_i(\mathbf{r},0)\rangle\langle\psi_i(\mathbf{r},0)|, \tag{12}$$

where N is the number of occupied orbitals and $\psi_i(\mathbf{r},0)$ are the ground state orbitals. This projected CAP ensures that only excited electrons in the CAP region are absorbed.

In the presence of a non-local potential, such as the non-local pseudopotential, the conventional definition of current density, $\mathbf{J}_c=(e\hbar/2mi)[\psi^*(\mathbf{r},t)\nabla\psi(\mathbf{r},t)-\psi(\mathbf{r},t)\nabla\psi^*(\mathbf{r},t)]$,

does not satisfy current conservation, $\nabla\cdot \mathbf{J}_c = 0$. We, therefore, calculate the local current using the expression proposed by Ref. 57

$$\mathbf{J}(\mathbf{r},t) = -e\sum_i^N \int_\Omega d\mathbf{r}'\psi_i^*(\mathbf{r},t)\mathbf{v}(\mathbf{r},\mathbf{r}')\psi_i(\mathbf{r}',t), \tag{13}$$

where Ω is the volume of the simulation cell and $\mathbf{v}(\mathbf{r},\mathbf{r}')$ is the so called velocity operator, defined by

$$\mathbf{v}(\mathbf{r},\mathbf{r}') = \frac{-i\hbar}{m}\nabla\delta(\mathbf{r}-\mathbf{r}') + \frac{1}{i\hbar}\left[\mathbf{r}V_{nonlocal}(\mathbf{r},\mathbf{r}') - V_{nonlocal}(\mathbf{r},\mathbf{r}')\mathbf{r}'\right]. \tag{14}$$

Sub-5-nm-wide GNRs[3] are desired for field effect transistors (FET) devices[6] due to their large band gap. Using chemical methods, many sub-5-nm GNR-based devices have been fabricated and studied.[2,3] We have investigated H-terminated ZGNRs with a width of 1.5 nm, which is similar to that of recent experiments[2,3] and is also sufficiently wide for the study of local currents in the presence of a single vacancy. The geometric structures of the pristine and single-vacancy ZGNRs are optimized using the projector-augmented wave method implemented in the Python Atomic Simulation Environment until the atomic forces converge to <0.02 eV/Å. The Kohn-Sham equations are solved on a real-space grid with a uniform spacing of 0.25 Å along each spatial coordinate. The simulation cell is a rectangular box with dimensions $L_x \times L_y \times L_z = 60\,\text{Å} \times 25\,\text{Å} \times 10\,\text{Å}$. The ZGNR lies in the x-y plane, with the long side parallel to the x axis. The left and right electrode regions of the bias potential are defined by $x < -20$ Å and $x > 20$ Å, respectively. The origin lies at the center of the simulation box. The projected CAP potential, W, begins at 10 Å from the x boundaries of the simulation cell. The time step is given by $\delta t = 0.001$ fs. The real space real time computer code used in this calculations is developed by our group.[58]

III. RESULTS AND DISCUSSION

In this section, we shall investigate the current dynamics induced by a two-step bias potential in pristine and single-vacancy ZGNR graphene nanoribbons. Figure 1 shows the geometry of the pristine ZGNR. The three carbon vacancy sites (labeled 1, 2, and 3) are also marked on the pristine geometry. Vacancy 1 sits at the edge of the nanoribbon. Vacancies 2 and 3 lie in the middle of the nanoribbon and belong to sublattices A and B, respectively. The step potential ramps to its maximum (minimum) value of 0.05 V (-0.05 V) over 0.5 fs. The shape of the bias potential is shown in Fig. 1.

Figure 2 shows the time-dependent currents of the four ZGNRs, as induced by the bias potential. The current is obtained by integrating the current density over the plane perpendicular to the center of the graphene nanoribbon, i.e., $I = \int J_x(x=0,y,z)dydz$. In each case, the current strongly oscillates until $\approx$2 fs, after which the current approaches a steady state. The current remains steady until the end of the simulation at time, $t = 8$ fs. The initial oscillations, which are caused by the relatively short ramp time, have been observed in other time-dependent calculations.[48,59–61] In each simulation, the projected CAP absorbs <0.066 electrons. At $t = 0$, the pristine and single-vacancy ZGNRs have 1160 and 1156 electrons, respectively. The small number of absorbed electrons justifies the use of the projected CAP for low bias voltage.

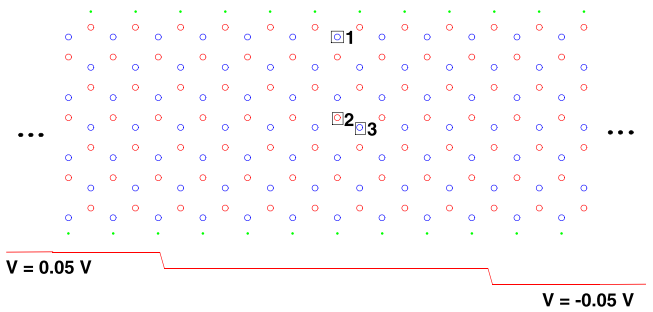

FIG. 1. Geometry of the pristine graphene nanoribbon in the region with zero complex absorbing potential. A (red) and B (blue) are the carbon atoms of the two sublattices. The hydrogen atoms (green) saturate the dangling carbon bonds. The three carbon vacancy sites (boxes 1, 2, and 3) are considered in the calculation; vacancy 1 is an edge vacancy, and vacancies 2 and 3 belong to sublattices A and B, respectively. The red line shows the change of the step potential along the x axis (the potential is constant in the perpendicular plane).

The pristine ZGNR current has, in general, the largest magnitude. The introduction of vacancies reduces the current, with a small drop in current for the edge vacancy and a large drop in current for vacancies near the center of the ZGNR. To understand why different vacancy positions result in considerably different conductance, we investigate the local current distribution of the defected ZGNRs.

We shall begin by describing the local currents of the pristine ZGNR at time, $t = 6$ fs, well within the steady-state regime. Figure 3(a) shows the vector flow of the local current along the plane of the pristine ZGNR. The x and y components of the current flow are obtained by integrating over the z direction

$$J_i = \int J_i(x,y,z)dz \quad i = x,y. \tag{15}$$

One observes that the current flows along the transport (x) direction and forms streamline patterns. The magnitude of

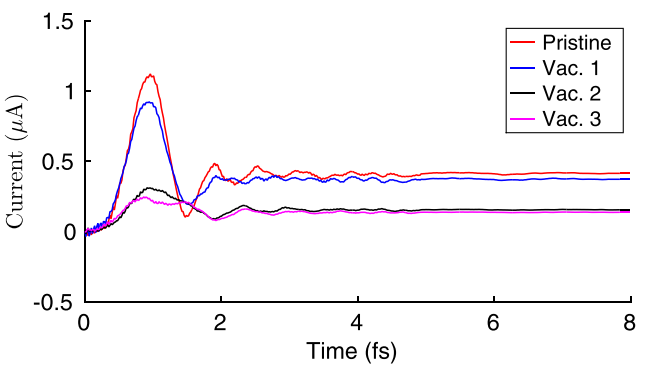

FIG. 2. Time-dependent current of the pristine ZGNR and the three single-vacancy GNRs (see Fig. 1).

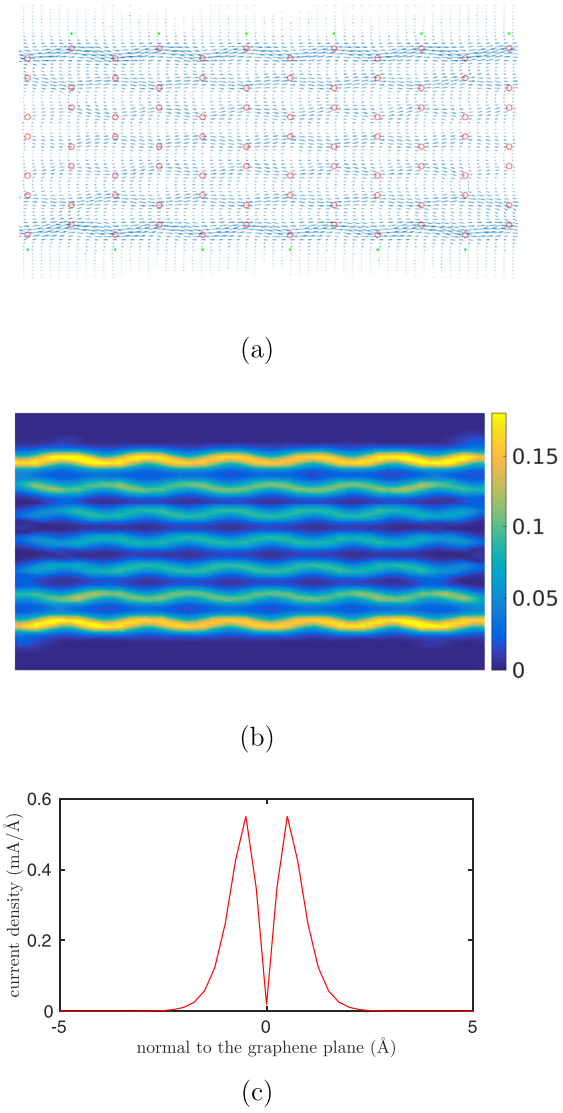

FIG. 3. Steady-state local current density of a pristine ZGNR. Each plot corresponds to time, $t = 6$ fs. Plot (a) shows a vector map of the local current parallel to the plane of the ZGNR, plot (b) shows the magnitude of the current density (units mA/Å), and plot (c) shows magnitude of current density in the direction perpendicular to the ZGNR plane.

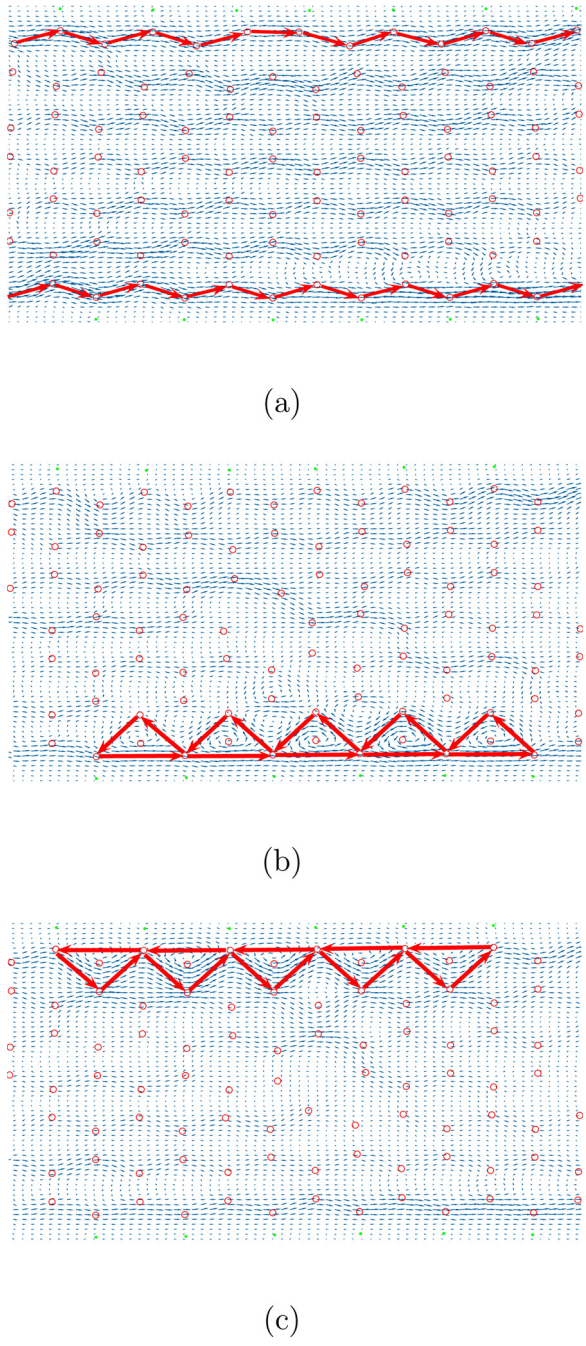

FIG. 4. Vector maps of the steady-state local current density parallel to the plane of a single-vacancy ZGNR at $t = 6$ fs. Plot (a) shows the local current for vacancy 1, which lies on the edge of the GNR. Plots (b) and (c) show the local current for vacancies 2 and 3, which are located in the middle on of the GNR on sublattices A and B, respectively. The three positions are shown in Fig. 1.

the current density is shown in Fig. 3(b). The current flow is greatest along the edge of the ZGNR since this region has a maximal density of states.[62] Fig. 3(c) shows the magnitude of the current density along the axis perpendicular to the middle of the ribbon (z axis), i.e., $\int J_x(0, y, z)dy$. The peak value is located at ≈0.5 Å above and below the ribbon plane, indicating that the current flow is dominated by π-bonded electrons. Due to the nodal symmetry of the π orbitals, the current flow splits into an upper and lower sheet.

We now turn to the description of the local current of the single-vacancy ZGNRs. Fig. 4(a) shows the local current distribution of a ZGNR with the edge vacancy. The edge current maintains the streamline pattern of a pristine ZGNR, and therefore, the conduction remains relatively high. The difference of ground and excited state electron density (not shown) is also the highest at the edges. Figs. 4(b) and 4(c) show that loop currents appear at the edge when a carbon vacancy is introduced in the middle of a ZGNR. The loop currents appear at sublattice A (B) when a vacancy is introduced in sublattice B (A). The carbon atoms which are adjacent to the vacancy, and are therefore the most affected, belong to the opposite sublattice. The loop currents, induced by the vacancies, break the streamline pattern, leading to the large drop in conductance. The current flow in the ZGNR is the result of the interference of all electron transport paths through the carbon lattice sites. Defects alter the transport path and, in some cases, induce loop currents. These loop currents can be quite pronounced (see the bottom of Fig. 4(b)

and the top of Fig. 4(c)), and in other cases, they are less visible (see the bottom left corner of Fig. 4(a)). By moving the position of the vacancy gradually from the edge to the center, the conductance decreases and the loop current at the edge increases.

IV. CONCLUSION

In conclusion, we studied the local current distribution of electrically biased ZGNRs using TDDFT. The calculations show that current mainly flows through the edge of pristine ZGNRs under small bias. Loop currents, due to electron hopping through carbon atoms belonging to the same sublattice, emerge at the ribbon edge when there is a carbon vacancy in the middle of ZGNRs. These loop currents hinder the flow of edge current, resulting in the poor electrical conductivity. Recent experiments have observed loop currents caused by electron backflow in graphene.[16] In our case, the loop currents are the result of electron hopping between carbon atoms belonging to the same symmetry sublattice. Neto *et al*. proposed that electrons in graphene could hop between carbon atoms belonging to the same sublattice, and that this hopping is very weak.[63] Our results show that inter-lattice hopping can be very strong under electrical bias when a carbon vacancy is introduced. These simulations will drive future experiments and simulations studying the effect of defects on the conductance of graphene nanoribbons. The projected CAP method has proven effective at low bias voltage. Simulations involving high bias voltages would be more complex since a method of electron injection would become necessary. Topics for future investigations include the local currents of multiple carbon vacancies, doped GNRs, and GNRs with surface adsorbates, which are common methods to modify the transport properties of GNRs.[64,65] The electron dynamics determine the performance of GNR-based devices, and therefore, studying local currents is important for developing practical applications of GNR-based device.

ACKNOWLEDGMENTS

This work has been supported by the National Science Foundation under Grant No. PHY-1314463.

[1]A. K. Geim, Science **324**, 1530 (2009).
[2]X. Wang, Y. Ouyang, X. Li, H. Wang, J. Guo, and H. Dai, Phys. Rev. Lett. **100**, 206803 (2008).
[3]X. Wang and H. Dai, Nat. Chem. **2**, 661 (2010).
[4]M. Y. Han, J. C. Brant, and P. Kim, Phys. Rev. Lett. **104**, 056801 (2010).
[5]W. S. Hwang, K. Tahy, X. Li, H. G. Xing, A. C. Seabaugh, C. Y. Sung, and D. Jena, Appl. Phys. Lett. **100**, 203107 (2012).
[6]P. B. Bennett, Z. Pedramrazi, A. Madani, Y.-C. Chen, D. G. de Oteyza, C. Chen, F. R. Fischer, M. F. Crommie, and J. Bokor, Appl. Phys. Lett. **103**, 253114 (2013).
[7]Q. Wang, R. Kitaura, S. Suzuki, Y. Miyauchi, K. Matsuda, Y. Yamamoto, S. Arai, and H. Shinohara, ACS Nano **10**, 1475 (2016).
[8]L. Vicarelli, S. J. Heerema, C. Dekker, and H. W. Zandbergen, ACS Nano **9**, 3428 (2015).
[9]Y.-C. Chen, T. Cao, C. Chen, Z. Pedramrazi, D. Haberer, G. de OteyzaDimas, F. R. Fischer, S. G. Louie, and M. F. Crommie, Nat. Nano **10**, 156 (2015).
[10]Y.-C. Chen, D. G. de Oteyza, Z. Pedramrazi, C. Chen, F. R. Fischer, and M. F. Crommie, ACS Nano **7**, 6123 (2013).
[11]Q. Peng, Y. Li, X. He, X. Gui, Y. Shang, C. Wang, C. Wang, W. Zhao, S. Du, E. Shi, P. Li, D. Wu, and A. Cao, Adv. Mater. **26**, 3241 (2014).
[12]L. Jiao, X. Wang, G. Diankov, H. Wang, and H. Dai, Nat. Nanotechnol. **5**, 321 (2010).
[13]D. V. Kosynkin, A. L. Higginbotham, A. Sinitskii, J. R. Lomeda, A. Dimiev, B. K. Price, and J. M. Tour, Nature **458**, 872 (2009).
[14]E. Ulrich Stützel, T. Dufaux, A. Sagar, S. Rauschenbach, K. Balasubramanian, M. Burghard, and K. Kern, Appl. Phys. Lett. **102**, 043106 (2013).
[15]A. Lubk, A. Béché, and J. Verbeeck, Phys. Rev. Lett. **115**, 176101 (2015).
[16]D. Bandurin, I. Torre, R. K. Kumar, M. B. Shalom, A. Tomadin, A. Principi, G. Auton, E. Khestanova, K. Novoselov, I. Grigorieva *et al*., Science **351**, 1055 (2016).
[17]T. Lehmann, D. A. Ryndyk, and G. Cuniberti, Phys. Rev. B **88**, 125420 (2013).
[18]S. M.-M. Dubois, A. Lopez-Bezanilla, A. Cresti, F. Triozon, B. Biel, J.-C. Charlier, and S. Roche, ACS Nano **4**, 1971 (2010).
[19]K. Saloriutta, A. Uppstu, A. Harju, and M. J. Puska, Phys. Rev. B **86**, 235417 (2012).
[20]J. E. Padilha, R. B. Pontes, A. J. R. da Silva, and A. Fazzio, Solid State Commun. **173**, 24 (2013).
[21]X. Deng, Z. Zhang, G. Tang, Z. Fan, and C. Yang, Carbon **66**, 646 (2014).
[22]B. G. Cook, W. R. French, and K. Varga, Appl. Phys. Lett. **101**, 153501 (2012).
[23]L. P. Zârbo and B. Nikolić, EPL **80**, 47001 (2007).
[24]J.-Y. Yan, P. Zhang, B. Sun, H.-Z. Lu, Z. Wang, S. Duan, and X.-G. Zhao, Phys. Rev. B **79**, 115403 (2009).
[25]G. C. Solomon, C. Herrmann, T. Hansen, V. Mujica, and M. A. Ratner, Nat. Chem. **2**, 223 (2010).
[26]J. Wilhelm, M. Walz, and F. Evers, Phys. Rev. B **89**, 195406 (2014).
[27]C. Cao, L. Chen, W. Huang, and H. Xu, Open Chem. Phys. J. **4**, 1 (2012).
[28]E. Runge and E. K. U. Gross, Phys. Rev. Lett. **52**, 997 (1984).
[29]S. Datta, *Electronic Transport in Mesoscopic Systems* (Cambridge University Press, 1997).
[30]Y. Xue, S. Datta, and M. A. Ratner, J. Chem. Phys. **115**, 4292 (2001).
[31]M. Di Ventra, *Electrical Transport in Nanoscale Systems* (Cambridge University Press, 2008).
[32]W. Kohn and L. J. Sham, Phys. Rev. **140**, A1133 (1965).
[33]G. Stefanucci and C.-O. Almbladh, EPL **67**, 14 (2004).
[34]G. Stefanucci and C.-O. Almbladh, Phys. Rev. B **69**, 195318 (2004).
[35]S. Kurth, G. Stefanucci, C.-O. Almbladh, A. Rubio, and E. K. U. Gross, Phys. Rev. B **72**, 035308 (2005).
[36]X. Zheng, F. Wang, C. Y. Yam, Y. Mo, and G. Chen, Phys. Rev. B **75**, 195127 (2007).
[37]S.-H. Ke, R. Liu, W. Yang, and H. U. Baranger, J. Chem. Phys. **132**, 234105 (2010).
[38]M. D. Ventra and T. N. Todorov, J. Phys.: Condens. Matter **16**, 8025 (2004).
[39]J. Maciejko, J. Wang, and H. Guo, Phys. Rev. B **74**, 085324 (2006).
[40]J. Yuen-Zhou, D. G. Tempel, C. A. Rodríguez-Rosario, and A. Aspuru-Guzik, Phys. Rev. Lett. **104**, 043001 (2010).
[41]C.-L. Cheng, J. S. Evans, and T. Van Voorhis, Phys. Rev. B **74**, 155112 (2006).
[42]A. Prociuk and B. D. Dunietz, Phys. Rev. B **78**, 165112 (2008).
[43]N. Sai, N. Bushong, R. Hatcher, and M. Di Ventra, Phys. Rev. B **75**, 115410 (2007).
[44]G. Stefanucci, S. Kurth, A. Rubio, and E. K. U. Gross, Phys. Rev. B **77**, 075339 (2008).
[45]S. Weiss, J. Eckel, M. Thorwart, and R. Egger, Phys. Rev. B **77**, 195316 (2008).
[46]P. Myöhänen, A. Stan, G. Stefanucci, and R. van Leeuwen, Phys. Rev. B **80**, 115107 (2009).
[47]X. Qian, J. Li, X. Lin, and S. Yip, Phys. Rev. B **73**, 035408 (2006).
[48]K. Varga, Phys. Rev. B **83**, 195130 (2011).
[49]C. A. Ullrich, *Time-Dependent Density-Functional Theory: Concepts and Applications* (Oxford University Press, Oxford, UK, 2012).
[50]N. Troullier and J. L. Martins, Phys. Rev. B **43**, 1993 (1991).
[51]J. P. Perdew and A. Zunger, Phys. Rev. B **23**, 5048 (1981).
[52]A. Castro, M. A. Marques, and A. Rubio, J. Chem. Phys. **121**, 3425 (2004).
[53]J. A. Driscoll, B. Cook, S. Bubin, and K. Varga, J. Appl. Phys. **110**, 024304 (2011).
[54]S. Bubin, B. Wang, S. Pantelides, and K. Varga, Phys. Rev. B **85**, 235435 (2012).
[55]A. Russakoff, S. Bubin, X. Xie, S. Erattupuzha, M. Kitzler, and K. Varga, Phys. Rev. A **91**, 023422 (2015).
[56]D. E. Manolopoulos, J. Chem. Phys. **117**, 9552 (2002).

[57]S. A. Sato and K. Yabana, Phys. Rev. B **89**, 224305 (2014).
[58]J. A. Driscoll and K. Varga, *Computational Nanoscience* (Cambridge University Press, 2010).
[59]B. Wang, Y. Xing, L. Zhang, and J. Wang, Phys. Rev. B **81**, 121103 (2010).
[60]C. Yam, X. Zheng, G. Chen, Y. Wang, T. Frauenheim, and T. A. Niehaus, Phys. Rev. B **83**, 245448 (2011).
[61]L. Zhang, J. Chen, and J. Wang, Phys. Rev. B **87**, 205401 (2013).
[62]Y.-W. Son, M. L. Cohen, and S. G. Louie, Phys. Rev. Lett. **97**, 216803 (2006).
[63]A. H. Castro Neto, F. Guinea, N. M. R. Peres, K. S. Novoselov, and A. K. Geim, Rev. Mod. Phys. **81**, 109 (2009).
[64]B. Huang, Z. Li, Z. Liu, G. Zhou, S. Hao, J. Wu, B.-L. Gu, and W. Duan, J. Phys. Chem. C **112**, 13442 (2008).
[65]H. Wang, T. Maiyalagan, and X. Wang, ACS Catal. **2**, 781 (2012).